Correlated multielectron systems in strong laser fields: A multiconfiguration time-dependent Hartree-Fock approach

J. Caillat,[1] J. Zanghellini,[1,2] M. Kitzler,[1,2] O. Koch,[3] W. Kreuzer,[3] and A. Scrinzi[1,*]
[1]*Photonics Institute, Vienna University of Technology Gusshausstrasse 27/387, A-1040 Vienna, Austria*
[2]*Center of Photonics Research, University of Ottawa, 150 Louis Pasteur Street, Ottawa, ON, KIN 6N5 Canada*
[3]*Institute for Analysis and Scientific Computing, Vienna University of Technology, Wiedner Hauptstrasse 8-10, A-1040 Vienna, Austria*
(Received 14 September 2004; published 21 January 2005)

The multiconfiguration time-dependent Hartree-Fock approach for the description of correlated few-electron dynamics in the presence of strong laser fields is introduced and a comprehensive description of the method is given. Total ionization and electron spectra for the ground and first excited ionic channels are calculated for one-dimensional model systems with up to six active electrons. Strong correlation effects are found in the shape of photoelectron peaks and the dependence of ionization on molecule size.

DOI: 10.1103/PhysRevA.71.012712 PACS number(s): 32.80.Fb, 32.80.Hd

I. INTRODUCTION

Electronic motion in the valence shell of atoms and molecules is becoming directly observable through newly developed radiation sources. These sources unite high intensities with short pulse durations and cover the wavelength range from the near infrared to the x-ray regime. Pulse durations extend from the picosecond range at modern synchrotron sources, over a few femtoseconds in few-cycle laser pulses, and similar time scales of radiation bunches in free electron lasers all the way to attosecond pulses of high-harmonic radiation generated by lasers. With time resolutions well below 1 fs, one may observe the rapid rearrangement of electron distributions in atomic relaxation processes [1], it may be possible to follow the transfer of charge along a larger molecule or to time-resolve the process of tunnel ionization in a strong electric field. It was shown that one may not only observe electronic motion, but also control it by the strong and well-defined electrical field of few-cycle laser pulses [2,3], which can be exploited, e.g., for imaging molecular structure by "microbunches" of coherent electrons [4] or for the selective excitation of atoms or molecules.

Theory must yet catch up with the new experimental possibilities. Much of our present understanding of valence electron motion is phrased in terms of a limited number of stationary states of the system and transitions between them. This approach makes reference to a large body of theory, which was primarily developed for traditional, time-independent spectroscopy and which relies to a great extent on numerical calculations of electronic structure. When a large number of states is involved, such a description becomes increasingly complex. Time-dependent "quantum interferences" between the states, which produce the dynamic behavior of the total wave function, become difficult to interprete and provide little insight into the physical processes. When continuum states become involved beyond lowest-order perturbative transitions, the stationary-state picture usually breaks down. In these cases an explicitly time-dependent approach may provide a more adequate or even the only viable theoretical description of electronic dynamics. This has long been recognized in strong laser-matter interactions, where external fields are comparable to the binding electric fields of the system and continuum states contribute dominantly. A similar situation arises when we calculate electronic motion in larger molecules, where the level spacing is small compared to the interaction energies involved. The situation is somewhat analogous to molecular wave packet dynamics, where a large number of involved states (bound or continuum) favors a time-dependent description over a picture of complex, time-dependent interferences between time-independent states [5].

Solving the time-dependent Schrödinger equation (TDSE) for a single electron in three spatial dimensions now has become a routine task that for most purposes can be solved easily. The interaction of multielectron systems with strong fields has been successfully modeled by the "single-active-electron" (SAE) approximation, where only a single electron is assumed to participate in the dynamics. This model provides our basic understanding of processes like high-harmonic generation in noble gases or (single) photoionization. When applied to molecules, however, the model turned out to be unreliable [6–9].

When two electrons are involved in the dynamics, a direct discretization of the TDSE becomes a formidable computational task requiring a maximum of available computer resources. Such computations were performed mostly to study the process of nonsequential double ionization of helium [10–13]. An extension of this approach to more than two electrons seems to be out of question and even in the two-electron case no definite results on nonsequential ionization could be provided so far. Similarly, multielectron calculations of molecules in strong fields have remained limited to H_2 [14–16].

An alternative method, which, in principle, could give exact results at low computational cost, is time-dependent density functional theory (TDDFT). Density functional theory has been most successfully applied to stationary many-electron states in solids. In its time-dependent, few-electron version it has encountered severe fundamental [17]

*Electronic address: scrinzi@tuwien.ac.at

and practical problems [18]. One problem is that TDDFT provides only the electron density, not the wave function, of the system, which makes it difficult to define observables, even such seemingly simple ones like photoelectron spectra. Possibly the most severe drawback of TDDFT is that it is difficult to systematically construct the all-important exchange-correlation potential V_{xc} or to estimate the accuracy of a given V_{xc}. Proposed methods for the construction of V_{xc} (e.g., [19,20]) seem to become as complex as more traditional ways of solving the TDSE.

Another popular method with low computational cost is the time-dependent Hartree-Fock (TDHF) approach. Early attempts to apply it to laser-matter interactions soon turned out to be futile as the very nature of laser excitation and ionization is incompatible with the TDHF ansatz [21]. This is easy to see by the following argument: In its simplest form the spatial HF wave function for a singlet two-electron system in its ground state is the product of two identical orbitals:

$$\Psi_0(\vec{r}_1,\vec{r}_2;t) = \phi(\vec{r}_1;t)\phi(\vec{r}_2;t). \tag{1}$$

When the system is ionized, one needs two different, orthogonal orbitals describing the ionic core and the detached electron, respectively:

$$\Psi_1(\vec{r}_1,\vec{r}_2;t) = \phi_1(\vec{r}_1;t)\phi_2(\vec{r}_2;t) + \phi_2(\vec{r}_1;t)\phi_1(\vec{r}_2;t). \tag{2}$$

In the ionization process, the TDHF wave function must undergo a transition from Ψ_0 to Ψ_1, which cannot happen in a continuous way during time evolution. This fundamental limitation may be overcome by going from "restricted" TDHF, where orbitals must be either identical or orthogonal, to "unrestricted" TDHF without constraints on ϕ_1 and ϕ_2 [22]. Although qualitative improvements using unrestricted TDHF were reported, satisfactory accuracies could not be reached [23].

There is evidence that inclusion of correlation by using a linear combination of several products $\phi_{j_1}\phi_{j_2}$ can produce rapidly convergent results. In Ref. [24] it was found that adding the field-free initial state $\psi_0(\vec{r}_1,\vec{r}_2)$ to the ansatz (2),

$$\Psi(\vec{r}_1,\vec{r}_2;t) = \psi_0(\vec{r}_1,\vec{r}_2) + \phi_1(\vec{r}_1;t)\phi_2(\vec{r}_2;t) + \phi_2(\vec{r}_1;t)\phi_1(\vec{r}_2;t), \tag{3}$$

provides field ionization yields for helium with accuracies on the level of a few percent for all relevant electric field strengths.

The multiconfiguration time-dependent Hartree-Fock (MCTDHF) method introduced in this work is a systematic extension of the (restricted or unrestricted) TDHF method. It is designed to close the gap between the in principle accurate, but computationally extremely demanding direct discretization of the time-dependent Schrödinger equation and methods like SAE, TDHF, or TDDFT, which do not provide satisfactory results for correlated multielectron systems and which cannot be improved systematically. We will show that not only in principle, but also in practice, converged single-electron spectra and ionization yields with up to six active electrons can be obtained with moderate computational effort.

The present development of the MCTDHF method is based on the multiconfiguration time-dependent Hartree (MCTDH) method for the propagation of wave packets. The MCTDH method was first introduced in 1990 [25,26] and has been applied to such diverse phenomena as absorption and photodissociation of small molecules [26–28], reactive scattering of hydrogen molecules [29], or the spin-boson model [30] (see Ref. [31] for a more complete list of applications). MCTDHF formally differs from MCTDH only by the exact exchange symmetry of the time-dependent Hamiltonian and the restriction on the subspace of totally antisymmetric solutions as well as by the two-particle nature of the electron-electron interaction. The resulting important technical differences between the methods will be pointed out below.

The paper is organized as follows: We define the method and summarize the derivation of the main equations. The most important aspects of an efficient computational implementation are discussed. Several technical issues are treated in appendixes. The method is applied to demonstrate the important role of electron correlation even in the simplest multielectron molecules, leading not only to quantitative, but even to qualitative differences in the ionization behavior.

II. THEORY

A. MCTDHF ansatz

In Hartree-Fock methods the full f-electron wave function $\Psi(q_1,\ldots,q_f)$ is approximated in terms of products of single-electron orbitals $\phi_j(q_i)$. For the ease of discussion of antisymmetry we use generalized coordinates $q_i=(s_i,\vec{r}_i)$ consisting of spin $s_i=\pm 1/2$ and spatial coordinates $\vec{r}_i \in \mathcal{R}^3$ of the ith electron. Antisymmetry of $\Psi(q_1,\ldots,q_f)$ with respect to interchange of any two of its arguments requires that $f!$ such products of single-electron orbitals be linearly combined in a Slater determinant:

$$\Phi(q_1,\ldots,q_f) = \frac{1}{\sqrt{f!}} \sum_{j_1=1}^{f} \cdots \sum_{j_f=1}^{f} \epsilon_{j_1\cdots j_f} \phi_{j_1}(q_1)\cdots\phi_{j_f}(q_f), \tag{4}$$

where $\epsilon_{j_1\cdots j_f}$ is fully antisymmetric—i.e., it changes sign under exchange of any two of its indices—and it is normalized by $\epsilon_{1\cdots f}=1$. The usual Hartree-Fock ansatz employs only a single Slater determinant or "configuration." The *multiconfiguration* Hartree-Fock ansatz used here consists of the linear combination of all Slater determinants that can be formed from N linearly independent orbitals ϕ_j:

$$\Psi_{\mathrm{MCHF}}(q_1,\ldots,q_f) = \frac{1}{\sqrt{f!}} \sum_{j_1=1}^{N} \cdots \sum_{j_f=1}^{N} B_{j_1\cdots j_f} \phi_{j_1}(q_1)\cdots\phi_{j_f}(q_f). \tag{5}$$

The coefficients $B_{j_1\cdots j_f}$ are assumed to be antisymmetric with respect to their indices, which leaves only $\binom{N}{f}$ independent B's. All other coefficients are either zero or differ only by a sign. In electronic structure calculations optimal B's and ϕ's are determined by minimizing the expectation value of the f-electron Hamiltonian H:

$$E_{\mathrm{MCHF}} = \min(\langle \Psi_{\mathrm{MCHF}}|H|\Psi_{\mathrm{MCHF}}\rangle). \tag{6}$$

A Galerkin condition is valid at the variational optimum,

$$\langle \delta\Psi_{\mathrm{MCHF}}|H|\Psi_{\mathrm{MCHF}}\rangle = 0, \tag{7}$$

where $\delta\Psi_{\mathrm{MCHF}}$ runs through all vectors in the tangent space at Ψ_{MCHF}—i.e., all functions $\tilde{\Psi}_{\mathrm{MCHF}} - \Psi_{\mathrm{MCHF}}$ where $\tilde{\Psi}_{\mathrm{MCHF}}$ is obtained from Ψ_{MCHF} by small variations $B_{j_1\cdots j_f} + \delta B_{j_1\cdots j_f}$ and $\phi_{j_i} + \delta\phi_{j_i}$. "Small" here means that only the lowest order in δ is retained. Condition (7) leads to the well-known multiconfiguration Hartree-Fock equations [32].

In MCTDHF the linear coefficients $B_{j_1\cdots j_f}(t)$ and the orbitals $\phi_{j_i}(q_i;t)$ are all assumed to be time dependent. Instead of the variational principle (7) one uses

$$\left\langle \delta\Psi_{\mathrm{MCHF}}(t) \left| i\frac{d}{dt} - H(t) \right| \Psi_{\mathrm{MCHF}}(t) \right\rangle = 0 \quad \forall\, t, \tag{8}$$

which ensures that the approximation is optimal in the *short-time* limit. Note that this does not mean that we obtain the best approximation to the exact solution at every single time t, but only that at any time t the derivative of the MCTDHF wave function, $id/dt\Psi_{\mathrm{MCHF}}(q_1,\ldots,q_f;t)$ is closest to its correct value $H(t)\Psi_{\mathrm{MCHF}}(q_1,\ldots,q_f;t)$ within the ansatz (5) [33].

For the further discussion we drop the label MCHF and denote the time-dependent MCHF wave function as Ψ.

B. Equations of motion

The derivation of equations of motion for the B's and ϕ_j's is greatly simplified by observing that we do not need to explicitly enforce antisymmetry during propagation. The fact that the Hamiltonian is fully symmetric under exchange of any two of the particles ensures that an initially antisymmetric state $\Psi(q_1,\ldots,q_f;0)$ remains antisymmetric during time propagation. Therefore, the equations of motion for the MCTDHF method are identical to those for the (nonsymmetric) MCTDH method developed for the propagation of nuclear wave packets [31]. The only difference is that in the exchange-symmetric case the equations become highly redundant, which must be taken into account for an efficient implementation. In the following we only briefly summarize the derivation of the equations of motion. For details we refer the reader to the review article on MCTDH [31].

Before starting the derivation it is important to note that the ansatz (5) is not unique, as Ψ is invariant under transformations of the form

$$\phi_j \to \tilde{\phi}_j = \sum_{k=1}^{N} S_{jk}\phi_k, \tag{9}$$

$$B_{j_1\cdots j_f} \to \tilde{B}_{j_1\cdots j_f} = \sum_{k_1=1}^{N} \cdots \sum_{k_f=1}^{N} S^{-1}_{j_1k_1}\cdots S^{-1}_{j_fk_f} B_{k_1\cdots k_f}, \tag{10}$$

where $S(t)$ can be any invertible, possibly time-dependent $N\times N$ matrix. We introduce a first restriction on S by demanding that the orbitals be orthonormalized:

$$\langle \phi_j|\phi_k\rangle = \delta_{jk}, \tag{11}$$

which limits the choice of $S(t)$ to unitary matrices. The remaining freedom in $S(t)$ can be exploited to choose a convenient relation between the orbitals and their time derivatives in the form

$$-i\left\langle \frac{d\phi_j}{dt} \middle| \phi_k \right\rangle = \langle \phi_j|g(t)|\phi_k\rangle, \tag{12}$$

where $g(t)$ is any self-adjoint, possibly time-dependent operator, which also includes the choice $g\equiv 0$. Self-adjointness of $g(t)$ in condition (12) ensures that the orthonormalization (11) remains valid through all times. It is easy to see that changing the constraint operator $g(t)\to g(t)+f(t)$ generates the transformations (9) and (10) with matrices $S(t)$ that satisfy the differential equation $idS_{jk}/dt = \Sigma_l\langle\phi_j|f(t)|\phi_l\rangle S_{lk}$.

The explicit form of admissible variations in Eq. (8) is

$$\delta\Psi = \sum_{j_1\cdots j_f} C_{j_1\cdots j_f}\frac{\partial\Psi}{\partial B_{j_1\cdots j_f}} + \sum_{i=1}^{f}\sum_{j_i=1}^{N}\chi_{j_i}\frac{\delta\Psi}{\delta\phi_{j_i}}, \tag{13}$$

where $C_{j_1\cdots j_f}$ are arbitrary complex numbers and $\chi_j(q_i)$ are arbitrary functions from the same Hilbert space as the ϕ_{j_i}. The functional derivative of any particular product of ϕ's with respect to the orbital ϕ_{j_i} is defined as

$$\frac{\delta(\phi_{k_1}\cdots\phi_{k_f})}{\delta\phi_{j_i}} = \begin{cases} \phi_{k_1}\cdots\phi_{k_{i-1}}\phi_{k_{i+1}}\cdots\phi_{k_f} & \text{for } k_i = j_i, \\ 0 & \text{otherwise.} \end{cases} \tag{14}$$

Inserting Eq. (13) into Eq. (8) and using the constraints (11) and (12) one obtains the following set of "working equations" for the time derivatives:

$$i\dot{B}_{j_1\cdots j_f} = \sum_{k_1\cdots k_f}\langle\phi_{j_1}\cdots\phi_{j_f}|H|\phi_{k_1}\cdots\phi_{k_f}\rangle B_{k_1\cdots k_f} - \sum_{i=1}^{f}\sum_{k=1}^{N}\langle\phi_{j_i}|g|\phi_k\rangle B_{j_1\cdots j_{i-1}kj_{i+1}\cdots j_f}, \tag{15}$$

$$i\dot{\phi}_j = g\phi_j + (1-P)\left[\sum_k\sum_l(\rho^{-1})_{jl}\overline{H}_{lk}\phi_k - g\phi_j\right]. \tag{16}$$

Here ρ_{jl} denotes the density matrix,

$$\rho_{jl} = \sum_{j_2=1}^{N}\cdots\sum_{j_f=1}^{N} B^*_{jj_2\cdots j_f}B_{lj_2\cdots j_f}, \tag{17}$$

and $\overline{H}_{lk}$ is the matrix of mean-field operators:

$$\overline{H}_{l_1k_1} = \left\langle \frac{\delta\Psi}{\delta\phi_{l_1}} \middle| H \middle| \frac{\delta\Psi}{\delta\phi_{k_1}} \right\rangle. \tag{18}$$

P is the projector onto the space spanned by the time-dependent orbitals $\phi_j(q;t)$:

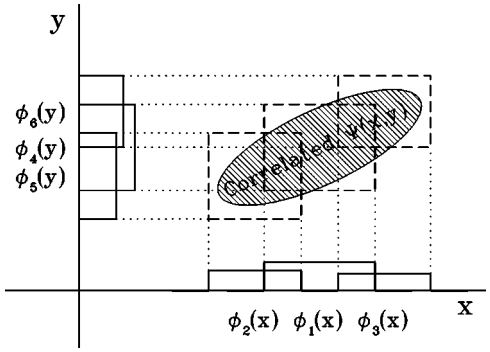

FIG. 1. Approximating a correlated wave function $\Psi(x,y)$ by a sum of products $\phi_j(x)\phi_l(y)$. The rectangles on the axes symbolize the individual ϕ's, and the dashed rectangles indicate the support of a single product. Several products are needed to cover the nonaligned support of Ψ.

$$P = \sum_{j=1}^{N} |\phi_j\rangle\langle\phi_j|. \tag{19}$$

The propagation equations also depend on the choice of the constraint operator g, which may be used to obtain different decompositions of the MCTDHF wave function Ψ (see Appendix A).

In Ref. [31] almost identical equations were derived except that in absence of antisymmetrization a different set of orbitals $\phi_j^{(i)}(q_i)$ may be used for each coordinate q_i. In the present case, where H is invariant under exchange of any two coordinates q_i and q_j and where also the initial state is antisymmetric, the orbitals and propagation equations are identical for all i.

The form of the equations of motion given here was used for the calculations presented in Refs. [34,35]. Recently a different derivation of the equations of motion was given in Ref. [36], where the method was applied to the hydrogen molecule in bound states.

C. Correlation

The single-configuration Hartree-Fock wave function is usually taken as the definition of an uncorrelated wave function. Improving the approximation by additional configurations therefore systematically introduces correlation into the ansatz until, in the limit of $N\to\infty$, the exact wave function is recovered. It is easy to see that the working equations turn into the ordinary Schrödinger equation when the orbitals ϕ_j form a complete set in the single-particle Hilbert space. In that case the projector $1-P$ is $\equiv 0$. With the particular choice $g\equiv 0$ the time derivatives of the orbitals (16) vanish and Eq. (15) turns into the exact TDSE represented in a basis of products of ϕ_j's.

Figure 1 illustrates how a correlated two-particle wave function $\Psi(x,y;t=0)$ is approximated by a sum of products of uncorrelated functions. For simplicity, antisymmetrization is disregarded. Uncorrelated functions then have the product form $\phi_j(x;t=0)\phi_k(y;t=0)$. Correlation manifests itself by the fact that the wave function Ψ is not aligned with the coordinate axes, while the product functions $\phi_j\phi_k$ are always aligned with the axes. Approximating the nonaligned Ψ requires adding products $\phi_j\phi_k$ until Ψ is covered. During time evolution $\Psi(x,y;t)$ will change its location and shape in the (x,y) plane, as is easy to see in the case of laser ionization. The time-dependent orbitals $\phi(t)$ evolve such as to optimally cover $\Psi(t)$. Provided that the degree of correlation in $\Psi(x,y;t)$ does not increase, roughly the same number of time-adjusted orbitals $\phi_j(x;t)$ suffices at all times. This behavior must be compared with a straightforward discretization of the (x,y) plane, where a sufficiently fine mesh must be laid over the whole plane covering any place where the solution might ever move to. An adaptive multidimensional grid mitigates that problem but still does not provide any means to take advantage of the fact that the two-particle solution may be well approximated by a short sum of products of single-particle orbitals. This picture also shows the limitations of the MCTDHF method. When strongly correlated structures appear during time evolution, a large number N of orbitals is needed, which will lead to a very large expansion size $\binom{N}{f}$. Such a situation may arise in the case of nonsequential double ionization. Numerical studies in $1+1$ dimensions exhibit characteristic, rather narrow jets of two electron emission in directions that are not aligned with the independent particle coordinates [37]. Clearly, patching up such structures requires a large number of uncorrelated products.

For clarity, in Fig. 1 we show only three out of nine possible products of the ϕ_j as the remaining six "configurations" have nearly no overlap with Ψ and remain "unoccupied." Some efficiency may be gained by only propagating "occupied" configurations, although in the present implementation we always use all configurations that can be constructed from a given set of ϕ_j's.

Sometimes highly correlated systems can be well described by changing to more appropriate coordinates [38]. However, this approach is excluded within the MCTDHF method, as the orbitals must be strictly associated with the individual particles to maintain antisymmetry.

Turning the argument around, the lack of convergence of a given observable with increasing number of MCTDHF orbitals indicates that a strongly correlated wave function is needed as the MCTDHF representation is optimal in the sense of the variational principle (8).

From a mathematical point of view, the working equations (15) and (16) differ qualitatively from the TDSE, which they approximate, because they are nonlinear. This is a direct and inevitable consequence of using self-adaptive orbitals. Such nonlinearities arise whenever the discretization is dynamically adapted to a specific solution. As a consequence, the working equations violate the quantum mechanical superposition principle and ground and excited states may exhibit spurious interactions. These problems can be overcome by choosing a sufficient number of N orbitals to keep artifacts small and by enforcing mutual orthogonality of ground and excited states during propagation to avoid accumulation of errors (see below). An initial state can be obtained from Eqs. (15) and (16) by propagating in imaginary time. With the additional orthogonality constraint, imaginary time propagation can also be used to obtain low-lying excited states. Non-

linearity also poses technical problems, because the most efficient numerical time-propagation algorithms (e.g., split-step or Lanczos-Arnoldi propagators) in their usual implementation are only applicable to linear equations. One way of dealing with this problem is the so-called "variational splitting" [39] discussed in Appendix A.

D. Implementation of the working equations

The Hamiltonian of a system with f electrons in an external electric field has the form

$$H(t) = \sum_{l=1}^{f} \frac{1}{2}\left[\frac{1}{\mathrm{i}}\vec{\nabla}_l - e\vec{A}(t)\right]^2 + V_n(\vec{r}_l) + \sum_{k=l+1}^{f} V_{ee}(|\vec{r}_l - \vec{r}_k|), \tag{20}$$

where the interaction of the electrons with the field is written in velocity gauge and in dipole approximation. $\vec{A}(t)$ and e denote vector potential and electron charge, respectively. We use atomic units unless indicated otherwise. The nuclei in the system are fixed in space and generate the potential $V_n(\vec{r}_i)$ on the ith electron. The Coulomb repulsion of the electrons is $V_{ee}(|\vec{r}_i - \vec{r}_k|) = e^2/|\vec{r}_i - \vec{r}_k|$ in full three dimensions and some smoothed version of this for lower-dimensional models (see below).

The important differences between nuclear dynamics (MCTDH [31]) and electronic dynamics (MCTDHF) arise from symmetry on the one hand and from the fact that the electronic Hamiltonian (20) contains only single- and two-particle operators, whereas potentials in nuclear dynamics typically depend on several coordinates. Because of antisymmetry vector sizes for the B's remain small and propagation of Eq. (15) for fixed ϕ's is a routine numerical task. As at most two-particle operators are involved, calculation of the matrix elements is simplified.

We start with rewriting Eq. (15), taking into account the antisymmetry of the B's. For simplicity we consider the case with constraint operator $g \equiv 0$. We restrict the indices to increasing f-tuples $j_1 > \cdots < j_f$,

$$i\dot{B}_{j_1<\cdots<j_f} = \sum_{k_1<\cdots<k_f}\left[\sum_p \epsilon_{p(k_1\cdots k_f)}\langle\phi_{j_1}\cdots\phi_{j_f}|H|\phi_{k_1}\cdots\phi_{k_f}\rangle\right] \times B_{k_1<\cdots<k_f}, \tag{21}$$

where p runs through all permutations of $k_1 < \cdots < k_f$. The sum over p can be expressed as the matrix element between two Slater determinants by observing that because of the exchange symmetry of H,

$$\sum_p \epsilon_{p(k_1\cdots k_f)}\langle\phi_{j_1}\cdots\phi_{j_f}|H|\phi_{k_1}\cdots\phi_{k_f}\rangle = \frac{1}{f!}\sum_p \epsilon_{p(k_1\cdots k_f)}\sum_q \epsilon_{q(j_1\cdots j_f)}\langle\phi_{j_1}\cdots\phi_{j_f}|H|\phi_{k_1}\cdots\phi_{k_f}\rangle, \tag{22}$$

with q running through all permutations of $j_1 < \cdots < j_f$. We now can apply the well-known Slater rules [32] to evaluate the matrix elements. In particular, only those matrix elements are nonzero where at most two indices in the sets $j_1\cdots j_f$ and $k_1\cdots k_f$ are different.

The single-particle contribution to the mean-field operators $\overline{H}_{lk}$ can easily be evaluated. We collect all single-particle operators in

$$H^{(1)} = \sum_{m=1}^{f} H_0(\vec{r}_m;t), \tag{23}$$

with

$$H_0(\vec{r};t) = \frac{1}{2}\left[\frac{1}{\mathrm{i}}\vec{\nabla} - e\vec{A}(t)\right]^2 + V_n(\vec{r}). \tag{24}$$

Inserting $H^{(1)}$ into Eq. (18) and using the definition of the functional derivative (14) one sees that two different kinds of contributions to $\overline{H}_{lk}$ arise. The first one is due to the term $m=1$ in the sum (23) and has the form

$$\overline{H}^{(1)}_{lk} = \sum_{j_2=1}^{N}\cdots\sum_{j_f=1}^{N} B^*_{lj_2\cdots j_f}B_{kj_2\cdots j_f}H(\vec{r}_1) = \rho_{lk}H_0(\vec{r}_1;t), \tag{25}$$

with the density matrix elements ρ_{lk} [Eq. (17)]. The remaining contributions are scalar terms of the form

$$B^*_{lj_2j_3\cdots j_f}B_{kk_2j_3\cdots j_f}\langle\phi_{j_2}|H_0(\vec{r}_2;t)|\phi_{k_2}\rangle \tag{26}$$

and similar terms where the subscripts of B^* and B are simultaneously permuted, which add up to a matrix of scalars Q_{lk}. This contribution to $\overline{H}_{lk}$ has no effect on the working equations, as the linear combination of orbitals $\Sigma_k Q_{lk}\phi_k$ is annihilated by $1-P$, which projects onto the orthogonal complement of all ϕ_k's.

The computationally most demanding terms arise from the two-particle operators:

$$H^{(2)} = \sum_{m<n} V_{ee}(\vec{r}_m - \vec{r}_n). \tag{27}$$

The terms with $m=1$ are

$$\overline{H}^{(2)}_{lk} = (f-1)\sum_{k_2=1}^{N}\sum_{j_2=1}^{N}\cdots\sum_{j_f=1}^{N} B^*_{lj_2j_3\cdots j_f}B_{kk_2j_3\cdots j_f}\langle\phi_{j_2}|V_{ee}(|\vec{r}_1 - \vec{r}_2|)|\phi_{k_2}\rangle, \tag{28}$$

where the scalar product is taken over coordinate q_2. Because of antisymmetry of the B's the contributions from all $n=2,\ldots,f$ are identical and summation over n results in the factor $f-1$. All terms with $m>1$ only generate a scalar matrix that does not contribute to the working equations as in the case of the single-electron part $\overline{H}^{(1)}_{lk}$.

Exact evaluation of the orbital mean-field potentials

$$\overline{V}_{j_2k_2}(\vec{r}_1;t) = \langle\phi_{j_2}|V_{ee}(|\vec{r}_1 - \vec{r}_2|)|\phi_{k_2}\rangle \tag{29}$$

requires integration over $\vec{r}_2$ for every single point $\vec{r}_1$ at each time t. In order to perform these integrals efficiently, we approximate V_{ee} in the form

$$V_{ee}(|\vec{r}_1-\vec{r}_2|) \approx \sum_{m=1}^{M} U_m(\vec{r}_1)U_m(\vec{r}_2), \tag{30}$$

with typical expansion length $M\sim 100$. The accuracy of the approximation in different spatial domains can be controlled by a weight function on the coordinates $\vec{r}_1$ and $\vec{r}_2$ (see Appendix B). Approximating the electron-electron repulsion by a sum of products of single-electron potentials is consistent with the product structure of the MCTDHF wave function.

Note that on a discrete space $\vec{r}_k$, $k=1,\ldots,Q$, V_{ee} can be exactly represented by a $Q\times Q$ matrix and Eq. (30) becomes exact for $M=Q$. For large $|\vec{r}_1-\vec{r}_2|$ the expansion rapidly converges with M, much like a multipole approximation. Most of the terms are needed to improve accuracy at small interelectronic distances. Further details on the expansion and a discussion of its accuracy are given in Appendix B.

When H does not contain spin-dependent operators, the initial spin state remains conserved throughout propagation and spin symmetry does not need to be imposed on the basis.

E. Absorption of outgoing flux

The wave function strongly expands during interaction with the field because of ionization. As the remote parts of the wave function are not needed to determine typical observables such as ionization yield or dipole response, the spatial domain where the wave function is calculated can be limited to some inner part. Doing that one must ensure that no unphysical reflections occur at the boundary of that domain. Nonreflecting boundary conditions depend on the kinetic energy of the particle and therefore each spectral component of the wave function requires a separate condition. Strictly speaking, such nonreflecting boundary conditions depend on the complete wave function and cannot be implemented locally. In practice, it has been demonstrated [40–42] that the addition of a "complex absorbing potential" (CAP) $-\mathrm{i}W(\vec{r})$ to the single-particle operator H_0 can provide nearly reflectionless absorption. The function W is zero in some sufficiently large inner domain and smoothly grows to W_a at the boundary of the range where the orbitals ϕ are calculated. The strength W_a and the extension L_a are adjusted empirically to ensure sufficient absorption and to avoid reflections for a given physical situation. We have chosen

$$W(\vec{r}) = \frac{W_a}{2}\left[1-\cos\left(\pi\frac{|\vec{r}|-R_a}{L_a}\right)\right] \quad \text{for } |\vec{r}|>R_a. \tag{31}$$

A different approach to removing outgoing flux is to multiply Ψ by a mask function $\Pi_{m=1}^{f} M_\tau(\vec{r}_m)$ at time intervals τ, where $M_\tau(\vec{r}_m)$ is $\equiv 1$ in the inner domain and becomes small at the boundary. To make overall absorption independent from the choice of τ, the mask function must depend on τ. When one chooses the τ dependence in the form $M_\tau(\vec{r}) = \exp[-\tau W(\vec{r})]$, absorption with mask M_τ and application of the CAP $-\mathrm{i}W(\vec{r})$ are equivalent in the limit $\tau\to 0$. We use CAP's, as the method is straightforward to implement.

F. Electron spectra

One important observable that *does* depend on the wave function at large distances is the electron energy spectrum. Provided that electronic motion beyond a certain distance can be considered as free motion of independent electrons in the laser field, electron spectra *after* time propagation can be calculated by recording the flux through a surface at finite distance *during* time propagation, which allows the calculation of electron spectra, when outgoing flux is absorbed outside that surface.

The energy spectrum of detached electrons is the sum over contributions from all possible ionization channels c:

$$\sigma(\vec{k}) = \lim_{T\to\infty} \sum_c |b_c(\vec{k},T)|^2. \tag{32}$$

In Appendix C it is shown that the channel amplitudes $b_c(\vec{k},T)$ at large time T can be written as

$$b_c(\vec{k},T) = i\int_{-\infty}^{T} dt\langle c,\vec{k};t|W|\Psi(t)\rangle \tag{33}$$

if the time evolution of $\Psi(t)$ is calculated with the CAP $-\mathrm{i}W$. The time-dependent channel wave function has the product form

$$|c,\vec{k};t\rangle = \Phi_c(t)\chi_{\vec{k}}(q_f,t), \tag{34}$$

where for large t the function $\Phi_c(t)$ evolves into the ionic bound-state function of the given channel and $\chi_{\vec{k}}(q_f,t)$ tends to the single-electron scattering state for electron momentum $\vec{k}$. The channel wave function does not need to be antisymmetrized, as only its antisymmetric parts contribute to the matrix element in Eq. (33).

Equation (33) has an intuitive interpretation: the absorption zone plays the role of a fuzzy surface over which the wave function is depleted proportional to W. The part of the wave function that is absorbed is analyzed in terms of momentum and channel and is added to the corresponding spectral amplitude. As contributions from all times can interfere in each channel, they must be added to $b_c(\vec{k},t)$ with a relative phase that reflects the time evolution of the channel function.

The procedure is related to similar methods [43–45], where the spectrum $|b_c(\vec{k},t=\infty)|^2$ is given by the Fourier transform of an autocorrelation function of $\Psi(t)$. The important difference is that for a time-independent Hamiltonian the time evolution of $|c,\vec{k};t\rangle$ is given by a multiplication by the phase $\exp[-\mathrm{i}t(E_c+k^2/2)]$, whereas it is nontrivial in the time-dependent case. Therefore in the presence of a field integration over t does not lead to a Fourier transform, but to a more general integral transform (see Appendix C). In practice, $\Phi_c(t)$ and $\chi_{\vec{k}}(q_f,t)$ can be calculated in parallel with the calculation of $\Psi(t)$ and the integral $b_c(\vec{k},T)$ can be accumulated as the propagation proceeds.

It must be mentioned that the validity of Eq. (33) is limited to situations where double ionization remains small. A generalization to multiple ionization is not considered here.

G. Propagation of excited states

Because of the nonlinearity of the equations, it is difficult to obtain MCTDHF approximations to excited states that have the same symmetry as the ground state. Similarly, when

propagating two initially orthogonal (ground and excited) states Ψ_0 and Ψ_1, they may not remain orthogonal. Both problems can be solved by adding an orthogonality constraint during propagation.

The variational principle (8) can be generalized for two orthogonal states Ψ_0 and Ψ_1 in the form

$$\langle \delta\Psi_0 | id/dt - H|\Psi_0\rangle + \langle \delta\Psi_1 | id/dt - H|\Psi_1\rangle - \lambda\,\delta\langle\Psi_0|\Psi_1\rangle = 0, \tag{35}$$

where the Lagrange parameter λ is determined with the help of the explicit constraint $\langle\Psi_0|\Psi_1\rangle=0$. For two orthogonal states

$$\Psi_0 = \sum_{j_1\cdots j_f} B_{j_1\cdots j_f}\phi_{j_1}\cdots\phi_{j_f}, \tag{36}$$

$$\Psi_1 = \sum_{k_1\cdots k_f} C_{k_1\cdots k_f}\chi_{k_1}\cdots\chi_{k_f}, \tag{37}$$

one obtains from Eq. (35) the equations of motion

$$i\dot{B}_{j_1\cdots j_f;\lambda} = \mathrm{i}\dot{B}_{j_1\cdots j_f} - \lambda X_{j_1\cdots j_f}, \tag{38}$$

$$i\dot{\phi}_{j;\lambda} = \mathrm{i}\dot{\phi}_j - \lambda\sum_{l,k=1}^{N}(\rho^{-1})_{jl}d_{lk}\chi_k, \tag{39}$$

and analogously for C and χ. Here $\dot{B}_{j_1\cdots j_f}$ and $\dot{\phi}_l$ are the derivatives *without* orthogonality constraint given by Eqs. (15) and (16), respectively. The quantities X and the matrix d are given by

$$X_{j_1\cdots j_f} = \frac{1}{f}\sum_{k_1}\sum_{k_2<\cdots<k_f}\langle\varphi_{j_1}|\chi_{k_1}\rangle C_{k_1\cdots k_f}D(j_2\cdots j_f,k_2\cdots k_f), \tag{40}$$

$$d_{j_1k_1} = \sum_{j_2<\cdots<j_f}\sum_{k_2<\cdots<k_f}B^*_{j_1\cdots j_f}C_{k_1\cdots k_f}D(j_2\cdots j_f,k_2\cdots k_f), \tag{41}$$

with $D(j_2\cdots j_f,k_2\cdots k_f)\coloneqq\det(M)$ and $M_{mn}=\langle\varphi_{j_m}|\chi_{k_n}\rangle, m,n=2,\ldots,f$. For determining the Lagrange multiplier λ one writes the orthogonality constraint in the differential form

$$0 = \mathrm{d}/\mathrm{d}t\langle\Psi_0|\Psi_1\rangle = \langle\dot{\Psi}_1|\Psi_0\rangle + \langle\Psi_0|\dot{\Psi}_1\rangle \tag{42}$$

and substitutes Eqs. (36) and (37), as well as the derivatives (38) and (39). The scheme can be readily generalized to more than two mutually orthogonal states.

Field-free excited states can be obtained by imaginary time propagation, starting from a set of mutually orthogonal guess states. In this particular case, where the solutions are time independent, one does not need to propagate Ψ_0 and Ψ_1 simultaneously, but one can first obtain a good ground state Ψ_0 and then propagate Ψ_1 orthogonal to that Ψ_0.

H. Computer resource requirements

The main technical advantage of the MCTDHF method is the compactness of the multielectron wave function. For f particles, N orbitals, and a given representation of the orbital function by Q numbers, a total of $\binom{N}{f}+N\times Q$ complex numbers are needed to store the complete MCTDHF wave function. In one dimension storage questions are unimportant, but even in three dimensions with, say, $Q\approx 10^5$ and $N=10$, wave function storage remains on the scale of 10 MB. In the antisymmetric case the largest part of storage is for the orbitals, while the number of B's remains small. This is another important difference to the Hartree method, where the number of B's grows like N^f.

CPU time is dominated by the computation of the mean-field operators $\bar{H}_{kl}$ and here mostly by the two-electron terms. When V_{ee} is approximated by an M-term expansion of the form (30), calculation of the two-electron matrix elements for N orbitals scales as $Q\times M\times N^2$. Typical computation times for our present one-dimensional models with $Q\sim 1000$, $N\sim 10$, and $M\sim 50$ are a few hours on a 2-GHz PC, depending on accuracy and laser pulse parameters. A straightforward extension to higher dimensions would increase computation times by factors of $\sim$100, depending on the actual increase in Q, resulting in weeks of computation time on a PC. Note that for linearly polarized lasers the wave function expands mostly in the polarization direction, where one needs a large number of discretization points, while fewer points are expected to suffice in the transverse directions.

To achieve computation times on the scale of hours also in the three-dimensional case, both more powerful hardware and improved time-propagation algorithms are needed. The method can be implemented on parallel computers as the major part of the operations—differentiation, multiplication, and calculation of the integrals—can be performed locally on separate spatial regions. The nonlocality caused by the mean-field potential remains manageable as the action of the mean fields on remote parts of the wave function requires only few terms of the expansion (30). This is easy to understand by the analogy with a multipole expansion, where the range of multipole fields rapidly decreases with multipole order. Improvements of the present time-propagation scheme may be achieved by taking advantage of the different time scales on which mean-field potentials and single orbitals evolve with the aim of reducing the number of expensive recalculations of the mean-field potentials.

III. APPLICATIONS

A. Correlation effects in ionization

The ionization behavior of atoms and small molecules in strong laser fields has successfully been described in the SAE approximation. With larger molecules both experimental and numerical findings indicate that the SAE approximation fails [6,46,47]. In Ref. [46] it was argued on the basis of a mean-field model of the multielectron effects that polarization of the molecule may be responsible for the discrepancy between SAE and observed rates. Here we show that correlation plays a key role in the ionization of molecules.

In our calculations we use one-dimensional f-atomic-model molecules with the potentials

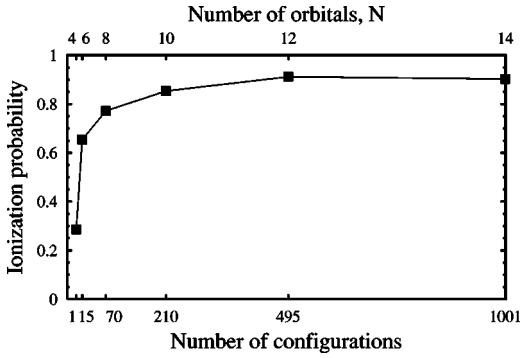

FIG. 2. Correlation dependence of the ionization yield for a four-atomic molecule with four active electrons exposed to a two-cycle laser pulse. The pulse parameters are wavelength 800 nm, pulse duration two optical cycle full width at half maximum (FWHM), trapezoidal pulse envelope, and peak intensity 4×10^{13} W/cm^2.

$$V_n(x) = -\sum_{k=1}^{f} \frac{1}{\sqrt{(X_k - x)^2 + a_f^2}}, \quad V_{ee}(|x-y|) = \frac{1}{\sqrt{(x-y)^2+1}}. \tag{43}$$

The atoms are assumed to be located at $X_k = 1.4[k-(f-1)/2]$ a.u. To facilitate comparison, the smoothing parameter a_f was adjusted for each f and N such that the ionization potential was the same for all molecules with a value of $I_p = 0.30$ a.u.

Figure 2 shows the correlation dependence of the ionization probability for the case $f=4$ going from single configuration ($N=4$) to 1001 configurations ($N=14$). A laser pulse with a central wavelength of 800 nm (photon energy 0.057 a.u.), duration of two cycles (FWHM of intensity), and peak intensity $I=4\times10^{13}$ W/cm^2 was used. The smoothing parameter a_f was slightly adjusted for each N to correct for the different correlation energies of the ion and neutral and keep the ionization potential $I_p=0.30$ with two-digit accuracy. The total ionization probability gradually increases from 30% in single configuration to a converged value of 89%. We see that correlation plays an important role during ionization. No meaningful result can be obtained with a single configuration. Although with 15 configurations ($N=6$) a big improvement towards the correct yield is made, satisfactory accuracy ($\sim$5%) is only reached with 210 configurations ($N=10$).

It was observed in [46] that molecule *size* is a key parameter for multielectron effects in ionization. Figure 3 illustrates that not only the absolute ionization yield, but also its change with molecule size is dependent on correlation. In Fig. 3(a) one sees the size dependence of ionization of molecules with between two and six active electrons obtained in Hartree-Fock approximation for a range of intensities. The result seems to confirm a naive expectation that larger molecules with correspondingly better polarizability should be easier to ionize. A similar result was published in [34]. This result is at variance with the conjecture that polarization should suppress (tunneling) ionization. However, when we improve our approximation by including correlation, the behavior reverses [Fig. 3(b)]: the molecules become *harder* to ionize with increasing size. It should be emphasized that this is a nontrivial effect of correlation, as the ionization potential was carefully kept constant at 0.30 a.u. for all molecules. Unfortunately, direct comparison of our results with Ref. [46] is difficult due to the very intuitive, but not systematic nature of the model used there. E.g., the electrons are not treated as identical particles with an antisymmetrized wave function and their mutual interactions are modeled only through the change of the overall electron density. In view of the high sensitivity of results to correlation, the qualitative agreement of the present result with the conclusions in Ref. [46] may be coincidental.

Recently, a one-dimensional (1D) single-configuration Hartree-Fock calculation of laser ionization of a model molecule with eight active electrons was reported [48], where a similar frequency dependence as in [46] was found. While seemingly this again confirms experimental findings, our result indicates that calculations on larger molecules cannot be trusted without a careful investigation of the importance of correlation.

B. Correlation in photoelectron spectra

Photoelectron spectra may be the single most important observable in laser-matter interactions, as they provide rich information about the dynamics of the whole system during ionization. The majority of attosecond physics experiments to date rely on the analysis of photoelectron and "above-threshold-ionization" (ATI) spectra. Exactly because spectra

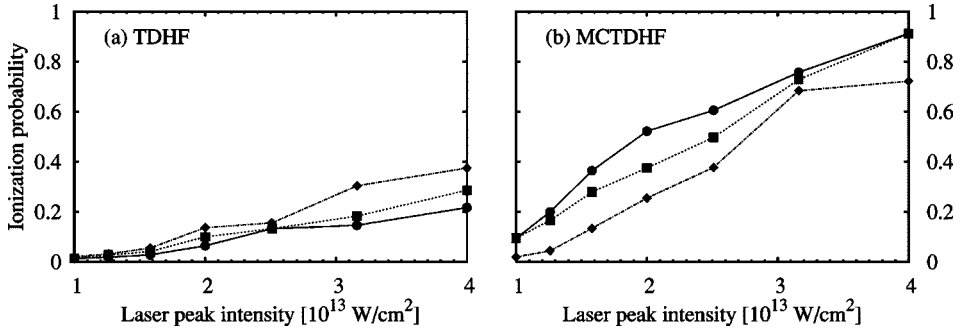

FIG. 3. Ionization probability for model molecules with two (circles), four (squares), and six (diamonds) active electrons calculated (a) in single configuration and (b) in multiconfiguration Hartree-Fock representation. Laser parameters as in Fig. 2, except for intensity.

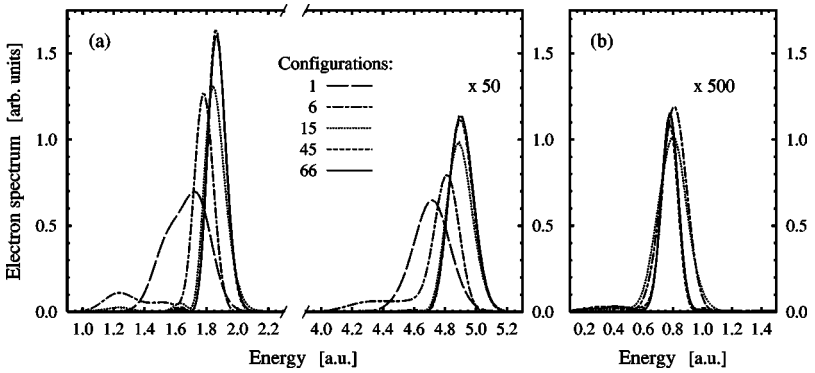

FIG. 4. Photoelectron peaks for ionization by a ten-cycle pulse at wavelength 15 nm for increasing number of configurations. (a) Channel where the ion remains in its ground state. Pulse peak intensity is $I=5\times10^{17}$ W/cm^2; the first and second ATI peak are shown. (b) Ion in the first excited state, $I=10^{16}$ W/cm^2.

depend in great detail on the dynamics leading to ionization, they constitute the most sensitive test for the accuracy of any calculation. Here we present electron spectra obtained from the MCTDHF method for (1+1)-dimensional He at short (15 nm) and long (800 nm) wavelengths and we investigate the importance of correlation for the spectral shape.

Figure 4(a) shows the photoelectron spectrum, when the ion remains in its ground state, for an increasing number of configurations. The electron-nucleus potential of our model atom is

$$V_n(x) = -\frac{2}{\sqrt{x^2+a^2}}, \tag{44}$$

with $a=\sqrt{2}/2$ a.u., which gives an ionization potential $I_p=1.21$ a.u. The vector potential of the pulse was assumed to be

$$A(t) = A_0 e^{-t^2/\tau^2}\sin(\omega t), \tag{45}$$

with $\omega=3.04$ a.u. ($\lambda=15$ nm) and $\tau=17.57$ a.u., which corresponds to ten optical cycles FWHM. A high intensity of 5×10^{17} W/cm^2 was chosen to obtain significant ionization. One sees that the peak obtained in single-configuration Hartree-Fock calculations is broadened towards lower energies. Qualitatively correct results start with a minimum of 15 configurations ($N=6$) and less than 2% accuracy of the first 2 ATI peak heights is reached with 45 configurations ($N=10$). This is consistent with the convergence behavior of the total yield reported earlier [35].

A similar unphysical broadening of the photoelectron peaks towards lower energies as in the single-configuration TDHF calculations was observed in TDDFT calculations. The tentative explanation for this observation given in Ref. [18] was that the superposition nature of a partially ionized state was not correctly reproduced by the calculation, but rather the action of the ionic core was screened by a fraction of the electron density remaining at the nucleus. Our results support this explanation.

Convergence is more difficult to obtain for excited ionic channels. Figure 4(b) shows the first peak of the first excited ionic channel at intensity $I=10^{16}$ W/cm^2 with all other parameters as above. Again a broadening of the peak is observed, when too few configurations are used. Moreover, the TDHF method ($N=2$, 1 configuration, not visible on the plot) fails to reproduce any ionization-excitation process. The first peak with a satisfactory shape is produced with 28 configurations ($N=8$) and accuracy of the peak height reaches better than 10% with 45 configurations ($N=10$).

A second set of calculations was performed at $\omega=0.057$ a.u. ($\lambda=800$ nm), $I=3\times10^{15}$ W/cm^2. Here a pulse duration of two optical cycle FWHM of intensity was chosen. The photoelectron spectra become very extended and no well-defined peak structure can be identified. Yet the electron spectra converge well (Fig. 5) with a convergence pattern similar as above, for the overall shape (a) as well as for the detailed structure (b). In this case we could not achieve satisfactory convergence for the excited ionic channel.

IV. CONCLUSIONS

At present the MCTDHF method is the only practical method to systematically study the dynamics of multielectron systems beyond simple essential state models. Its main advantages are the compact representation of the time-

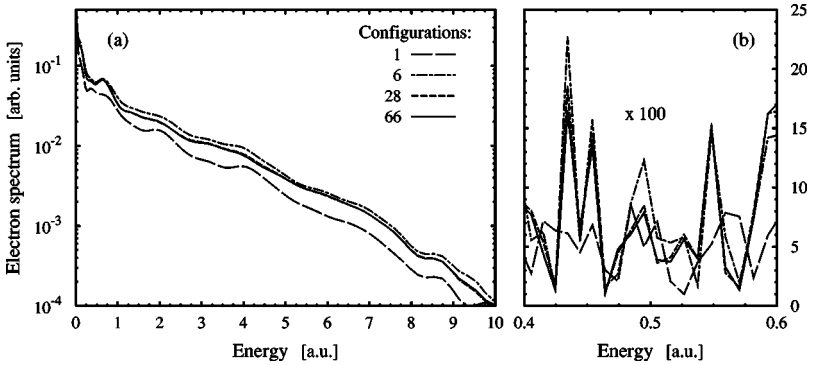

FIG. 5. Photoelectron spectrum for the ionic ground-state channel at wavelength 800 nm with increasing number of configurations: (a) whole energy range (the curves are smoothened for better visibility) and (b) details over a short energy range (without smoothing). Converged results are obtained from 28 configurations ($N\geqslant8$).

dependent multielectron wave function on the one hand and the full inclusion of correlation on the other hand. Alternative, in principle equally accurate methods using fixed basis sets (like CI) or meshes in the multiparticle configuration space require prohibitive computer storage and CPU times. Other methods are in principle (TDHF) or in present realizations (TDDFT) not capable to adequately describe excited states, superposition states, or correlations.

We have discussed the most important elements of the MCTDHF method: the basic ansatz, the equations of motion, the treatment of antisymmetry, the inclusion of spin, the calculation of excited initial states and their propagation in time, the calculation of electron spectra in presence of the electric field and absorbing potentials, and a systematic way of approximating the electron-electron potential. It was shown that in the limit of large expansion the method converges to the exact solution of the time-dependent Schrödinger equation. Convergence was demonstrated for ionization yields of 1D many-electron molecules and for electron spectra from a 1D two-electron atom.

The MCTDHF method is the method of choice to study the effects of correlation. Its limiting case of a single configuration is TDHF, which is usually taken as a definition of what is an uncorrelated method. By adding more configurations, correlation specific effects can be isolated. In our examples, we have shown that correlation plays an important role in the interaction of multielectron systems with strong laser fields. By comparing MCTDHF calculations with TDHF calculations we found that correlation is crucial for electron spectra and even robust observables such as the total ionization yield from molecules may change not only quantitatively, but even qualitatively when correlation is included.

The purpose of this work was to present the method and to demonstrate its feasibility using one-dimensional multielectron models. Certain questions of laser-matter interactions may depend on the three dimensionality of space. A well-known example, where this may apply, is the "rescattering" of a detached electron with the parent ion under the influence of a strong laser field: in one dimension rescattering is nearly inevitable, whereas in three dimensions due to transverse wave packet spreading only a small fraction of electrons will return to the nucleus. The MCTDHF method may be extended to three dimensions, as the computational effort grows with dimension like for a single-particle Schrödinger equation. However, at present it is difficult to predict how correlation—i.e., the number of Slater determinants required for convergence—scales with dimension. To clarify this question, a three-dimensional version of the presented code is currently being developed.

ACKNOWLEDGMENTS

We are indebted to H.-D. Meyer for introducing us to the MCTDH method and to Christian Lubich for several fruitful discussions. This work was supported by the Austrian Research Fund special research programs ADLIS (F016) and AURORA (F011).

APPENDIX A: TIME PROPAGATION

For the spatial discretization of our one-dimensional model systems we used an equidistant grid of Q points x_m on the interval $[-L,L]$. The derivatives were approximated in pseudospectral form as

$$\frac{\partial \Psi}{\partial x}(x_j) = \frac{1}{Q}\sum_{l,m=1}^{Q} (\mathrm{i}k_l) e^{\mathrm{i}k_l x_j} e^{-\mathrm{i}k_l x_m} \Psi(x_m), \quad k_l := \frac{\pi l}{L}, \tag{A1}$$

and analogously for $\partial^2/\partial x^2$. The discrete Fourier transforms were performed using standard fast Fourier transform (FFT) routines.

We tested two different forms of solving the working equations (15) and (16). As a first method we chose the constraint operator $g \equiv 0$ and united the complex values of $B_{j_1 \cdots j_f}$ and ϕ_j into a single vector, which was propagated using a variable order self-adaptive Runge-Kutta scheme. The error was controlled by the comparison of two steps with a single step of double size. The method showed no instabilities, and accuracy loss due to roundoff errors did not exceed three or four digits.

As a second method we implemented the "variational splitting" proposed in Ref. [39]. In that method one chooses the single-particle Hamiltonian (23) as the constraint operator $g(t)=H_0(t)$, which leads to the working equations

$$i\dot{B}_{j_1 \cdots j_f} = \sum_{k_1 \cdots k_f} \langle \phi_{j_1} \cdots \phi_{j_f} | H^{(2)} | \phi_{k_1} \cdots \phi_{k_f} \rangle B_{k_1 \cdots k_f}, \tag{A2}$$

$$i\dot{\phi}_j = H_0(t)\phi_j + (1-P)\left[\sum_k \sum_l \rho_{jl}^{-1} \bar{H}_{lk}^{(2)} \phi_k\right]. \tag{A3}$$

The mean-field operator is defined analogous to Eq. (18) with the full Hamiltonian H replaced by the two-particle Hamiltonian $H^{(2)}$ defined in Eq. (27). A split-step strategy was applied to solve this set of equations as follows:

(i) Compute $\phi_j^{(1)}$ by solving

$$i\frac{\mathrm{d}}{\mathrm{d}t}\phi_j(t) = H_0(t)\phi_j(t) \tag{A4}$$

for the interval $[t_0, t_0+\Delta t/2]$ with initial values $\phi_j(t_0)$.

(ii) Compute $B_{j_1 \cdots j_f}(t_0+\Delta t)$ and $\phi_j^{(2)}$ by solving Eqs. (A2) and (A3) for the interval $[t_0, t_0+\Delta t]$, where the term H_0 is omitted.

(iii) Compute $\phi_j(t_0+\Delta t)$ by integrating Eq. (A4) in the interval $[t_0+\Delta t/2, t_0+\Delta t]$ with the initial values $\phi_j^{(2)}$.

The algorithm is of second order in the time step Δt as the "constant mean-field" method used in the MCTDH method [49]. Here the procedure is used to separate integration of the single-particle orbitals from the complete set of equations, while in the MCTDH method is serves to separate the integration of the (very large) vector of B's.

The motivation for variational splitting is that H_0 contains the unbounded derivative operators, for which schemes like the explicit Runge-Kutta method are known to perform poorly. As unbounded terms are now isolated in the linear equation (A4), more efficient integrators can be employed. The operators of the remaining nonlinear equations were all bounded in our examples and may be efficiently integrated by explicit schemes.

The deeper physical reason for separating the single-electron Hamiltonian from the interaction is the fact that there are two rather different regimes of electronic motion: interaction between electrons, which is more important at lower velocities, and very rapid motion of the nearly free electron in the external field, during which electrons can be accelerated to very high momenta where large eigenvalues of the momentum and energy operators become involved.

An extensive comparison of the two methods [50] has shown that at the accuracies required for observables like ionization or electron energy spectra, a fourth-order Runge-Kutta outperforms the variational splitting method, with up to an order of magnitude fewer evaluations of the mean-field operators $\overline{H}$ in the Runge-Kutta scheme than evaluations of the analogous $\overline{H}^{(2)}$ in the variational splitting. A further analysis must show whether this is a fundamental limitation of the splitting method or whether it applies only for the present implementation and/or range of parameters.

APPENDIX B: APPROXIMATION OF V_{ee}

The approximation of V_{ee} in the form (30) is made in two steps: (a) discretization of V_{ee} and (b) lower-rank approximation of the resulting matrix.

We approximate V_{ee} using a set of local basis functions $\{|i\rangle, i=1,\ldots,L\}$ in the form

$$V_{ee} \approx V_{\mathrm{app}} = RVR = \sum_{i,i'=1}^{L} \sum_{j,j'=1}^{L} |i\rangle (Q^{-1})_{ij} \tilde{V}_{jj'} (Q^{-1})_{j'i'} \langle i'|, \tag{B1}$$

where the projectors R are given by

$$R = \sum_{i,j=1}^{L} |i\rangle (Q^{-1})_{ij} \langle j|, \quad Q_{ij} = \langle i|j\rangle. \tag{B2}$$

The discrete approximation matrix is

$$\tilde{V}_{ij} = \int d\vec{r} \int d\vec{r}\,' h_i(\vec{r}) V_{ee}(|\vec{r}-\vec{r}\,'|) h_j(\vec{r}\,'), \tag{B3}$$

where we chose real functions $h_i(\vec{r})$ as the basis functions $|i\rangle$. In general, a rather small number of basis functions $L \sim 100$ is used and the functions are denser inside the atom or molecule, where most electron-electron interactions are expected to take place. Typically, L is one or two orders of magnitude less than the number of discretization points for Φ.

For the second step we make a Schmidt decomposition of the matrix $\tilde{V}_{ij}$, which gives the optimal approximation by a lower-rank matrix in the L^2 sense [51]. In order to control local distribution of the error, we use a weighted overlap matrix

$$S_{ij} = \int d\vec{r} g(\vec{r}) h_i(\vec{r}) h_j(\vec{r}), \tag{B4}$$

where the weight function $g>0$ may emphasize certain regions. Let the columns of the matrix U denote the eigenvectors associated with eigenvalues u_m:

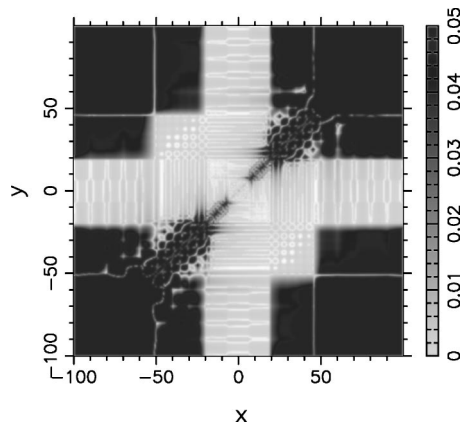

FIG. 6. Approximation of V_{ee} on a grid of 1000×1000 points by an operator of rank 55. The gray scale indicates the relative error $|V_{\mathrm{app}}-V_{ee}|/|V_{ee}|$ in the (x,y) plane.

$$\sum_{j=1}^{L} \tilde{V}_{ij} U_{jm} = \sum_{j=1}^{L} S_{ij} U_{jm} u_m. \tag{B5}$$

With the definition $\tilde{U} := SU$ the matrix $\tilde{V}$ now can be written as

$$\tilde{V} = \tilde{U} u \tilde{U}^T, \tag{B6}$$

where u denotes the diagonal matrix of eigenvalues. The eigenvectors are orthogonal and normalized with respect to $S: U^T S U = 1$. For simplicity we assume that all u_m are positive and that they are sorted in descending order. A lower-rank approximation of $\tilde{V}$ is obtained by setting $u_m = 0$ for all $m > M$. Our final approximation is now

$$V_{\mathrm{app}}(\vec{r}-\vec{r}\,') = \sum_{i,j=1}^{N} h_i(\vec{r}) \sum_{m=1}^{L} [Q^{-1}\tilde{U}]_{im}\, u_m [\tilde{U}^T Q^{-1}]_{mj}\, h_j(\vec{r}\,'). \tag{B7}$$

Because of the weight function g, the V_{app} is more accurate where $g(\vec{r})$ is large, usually near the atom or molecule. With the definition

$$U_m(\vec{r}) := \sqrt{u_m} \sum_{i=1}^{L} h_i(\vec{r}) [Q^{-1}\tilde{U}]_{im}, \tag{B8}$$

we obtain Eq. (30). The present method can be considered a special case for two-particle potentials of the more general procedure used in the MCTDH method [52] once the first step of mapping onto a coarser grid was made.

Figure 6 shows the relative accuracy of the approximation of the softened Coulomb potential (43). Here the grid for the $\phi_j(x)$ has 1000 points in the range $x \in [-100, 100]$, a number of $L=83$ unevenly spaced basis functions $|i\rangle$ were used, and the final rank of the approximation is $M=55$. The weight function was set to $g(x)=1$ for $x<6$ and decreased stepwise to $g(x)=0.1$ at $x=100$. In the inner cross-shaped region *relative* errors of the approximation remain below 1%.

APPENDIX C: ELECTRON SPECTRA

Here we derive Eq. (33) for the ionization channel amplitude. For simplicity we disregard the exchange symmetry of the wave function Ψ and the Hamiltonian.

Let us assume we have f electrons, of which the fth electron is detached by the field. We split the Hamiltonian without the CAP as follows:

$$\tilde{H} = H_0 + V_f, \quad H_0 := H_{\text{ion}} + T_f, \quad V_f := V_n^f + V_{ee}^f, \quad \text{(C1)}$$

where H_{ion} is the ionic Hamiltonian for $f-1$ electrons including the field, $T_f=[-i\vec{\nabla}_f - eA(t)]^2/2$ is the detached electron's kinetic energy including the quiver energy in the electric field, V_n^f is the nuclear potential for the fth electron, and

$$V_{ee}^f := \sum_{m=1}^{f-1} V_{ee}(|\vec{r}_m - \vec{r}_f|) \quad \text{(C2)}$$

is the interaction of the core with the fth electron.

For times T when the laser pulse is over, the ionization amplitude into channel c is

$$b_c(\vec{k},T) = \langle c,\vec{k};T|\tilde{\Psi}(T)\rangle. \quad \text{(C3)}$$

Here $\tilde{\Psi}(T)$ is the complete wave function (propagated without CAP) at time T. The scattering wave function for a given ionization channel c has the product form

$$|c,\vec{k};T\rangle = \Phi_c(T)\chi_{\vec{k}}(q_f,T), \quad \text{(C4)}$$

where we choose the time evolution

$$i\frac{d}{dt}\Phi_c(t) = H_{ion}(t)\Phi_c(t), \quad \text{(C5)}$$

with the boundary condition

$$H_{ion}(t)\Phi_c(t) = E_c\Phi_c(t) \quad \text{for } t > T, \quad \text{(C6)}$$

and

$$i\frac{d}{dt}\chi_{\vec{k}}(q_f,t) = T_f(t)\chi_{\vec{k}}(q_f,t), \quad \text{(C7)}$$

with the boundary condition

$$T_f(t)\chi_{\vec{k}}(q_f,t) = \frac{k^2}{2}\chi_{\vec{k}}(q_f,t) \quad \text{for } t > T. \quad \text{(C8)}$$

We now demonstrate that b_c only depends on the time evolution of the wave function on some surface $|\vec{r}_f|=R$. We write

$$\langle c,\vec{k};T|\tilde{\Psi}(T)\rangle \approx \langle c,\vec{k};T|\theta(|\vec{r}_f| - R)|\tilde{\Psi}(T)\rangle, \quad \text{(C9)}$$

where the step function is $\theta(x)=0$ for $x<0$ and $=1$ for $x>0$. R must be chosen large enough that any bound-state contribution to the channel c can be neglected and T must be large enough that all detached electrons with momentum $\vec{k}$ have moved beyond R. We write the right-hand side of (C9) as an integral over time:

$$\int_{-\infty}^{T}\left[\frac{d}{dt}\langle c,\vec{k};t|\theta(|\vec{r}_f| - R)|\tilde{\Psi}(t)\rangle\right]dt = \int_{-\infty}^{T} i\langle c,\vec{k};t|H_0\theta(|\vec{r}_f| - R) - \theta(|\vec{r}_f| - R)\tilde{H}|\tilde{\Psi}(t)\rangle. \quad \text{(C10)}$$

When we assume that $V_f \sim 0$ for $|\vec{r}_f|>R$, only the commutator $[T_f(t), \theta(|\vec{r}_f|-R)]$ contributes to the integral, which only depends on $\tilde{\Psi}^*(t)\nabla\tilde{\Psi}(t)$ on the surface $|\vec{r}_f|=R$.

Let us now introduce a CAP $-iW$ and replace in Eq. (C3) the exact solution $\tilde{\Psi}$ with the solution Ψ where the outgoing flux is absorbed by the CAP. At time T, when all detached electrons have moved beyond R and have been absorbed, we have

$$0 = \langle c,\vec{k};T|\Psi(T)\rangle \quad \text{(C11)}$$

$$= \int_{-\infty}^{T} i\langle c,\vec{k};t|[T_f,\theta(|\vec{r}_f| - R)] - iW|\Psi(t)\rangle. \quad \text{(C12)}$$

When the CAP is chosen such as not to alter the time evolution on the surface $|\vec{r}_f|=R$, the first term in the integral is the channel amplitude (C3). It exactly cancels with the second term, which gives Eq. (33).

Furthermore, for time-independent Hamiltonians, the time evolution of the channel functions is given by

$$|c,\vec{k};t\rangle = e^{-it(E_c+k^2/2)}|c,\vec{k};0\rangle. \quad \text{(C13)}$$

Substituting Eq. (C13) into Eq. (C3) and taking the modulus squared one obtains a twofold integral over time for the spectrum in channel c:

$$\sigma_c(\vec{k}) = \int_{-\infty}^{\infty} dt \int_{-\infty}^{\infty} dt' \langle\Psi(t)|W|c,\vec{k};0\rangle \times\langle c,\vec{k};0|W|\Psi(t')\rangle e^{-i(t-t')(E_c+k^2/2)}, \quad \text{(C14)}$$

where we have set the upper time limit to $T=\infty$. This expression can be rewritten as the Fourier transform of an autocorrelation function of $\Psi(t)$. A similar equation for the reactive scattering amplitude is given in Refs. [31,53]. When the Hamiltonian is time dependent, time evolution of the channel function becomes a general unitary transform and writing Eq. (C14) as a Fourier transform is no longer possible.

[1] M. Drescher, M. Hentschel, R. Kienberger, M. Uiberacker, V. Yakovlev, A. Scrinzi, T. Westerwalbesloh, U. Kleineberg, U. Heinzmann, and F. Krausz, Nature (London) **419**, 803 (2002).

[2] R. Kienberger *et al.*, Science **297**, 1144 (2002).

[3] E. Goulielmakis *et al.*, Science **305**, 1267 (2004).

[4] M. Spanner, O. Smirnova, P. Corkum, and M. Ivanov, J. Phys. B **37**, L243 (2004).

[5] E. J. Heller, Acc. Chem. Res. **14**, 368 (1981).

[6] M. Lezius, V. Blanchet, D. M. Rayner, D. M. Villeneuve, A. Stolow, and M. Y. Ivanov, Phys. Rev. Lett. **86**, 51 (2001).
[7] S. M. Hankin, D. M. Villeneuve, P. B. Corkum, and D. M. Rayner, Phys. Rev. Lett. **84**, 5082 (2000).
[8] V. R. Bhardwaj, P. B. Corkum, and D. M. Rayner, Phys. Rev. Lett. **91**, 203004 (2003).
[9] A. N. Markevitch, S. M. Smith, D. A. Romanov, H. B. Schlegel, M. Y. Ivanov, and R. J. Levis, Phys. Rev. A **68**, 011402(R) (2003).
[10] J. S. Parker, L. Moore, and K. Taylor, Opt. Express **8**, 436 (2001).
[11] P. Burke, J. Colgan, D. H. Glass, and K. Higgins, J. Phys. B **33**, 143 (2000).
[12] P. Lambropoulos, P. Maragakis, and J. Zhang, Phys. Rep. **305**, 203 (1999).
[13] A. Scrinzi and B. Piraux, Phys. Rev. A **58**, 1310 (1998).
[14] K. Harumiya, I. Kawata, H. Kono, and Y. Fujimura, J. Chem. Phys. **113**, 8953 (2000).
[15] A. Saenz, Phys. Rev. A **66**, 063407 (2002).
[16] K. Taylor, Phys. Scr. **T105**, 31 (2003).
[17] N. T. Maitra, K. Burke, and C. Woodward, Phys. Rev. Lett. **89**, 023002 (2002).
[18] V. Véniard, R. Taïeb, and A. Maquet, Laser Phys. **13**, 465 (2003).
[19] A. Görling and M. Levy, Phys. Rev. A **50**, 196 (1994).
[20] M. Seidl, J. P. Perdew, and S. Kurth, Phys. Rev. Lett. **84**, 5070 (2000).
[21] K. C. Kulander, Phys. Rev. A **36**, 2726 (1987).
[22] M. S. Pindzola, P. Gavras, and T. W. Gorczyca, Phys. Rev. A **51**, 3999 (1995).
[23] N.-E. Dahlen and R. van Leeuwen, Phys. Rev. A **64**, 023405/1 (2001).
[24] A. Scrinzi, Phys. Rev. A **61**, 041402(R) (2000).
[25] U. Manthe, H.-D. Meyer, and L. S. Cederbaum, J. Chem. Phys. **97**, 3199 (1992).
[26] H.-D. Meyer, U. Manthe, and L. S. Cederbaum, Chem. Phys. Lett. **165**, 73 (1990).
[27] L. Liu, J.-Y. Fang, and H. Guo, J. Chem. Phys. **102**, 2404 (1995).
[28] H. Köppel, M. Döscher, H.-D. Meyer M. I. Baldea, and P. Szalay, J. Chem. Phys. **117**, 2657 (2002).
[29] A. Jäckle and H.-D. Meyer, J. Chem. Phys. **102**, 5605 (1995).
[30] M. Thoss, H. Wang, and W. Miller, J. Chem. Phys. **115**, 2991 (2001).
[31] M. H. Beck, A. Jäckle, G. A. Worth, and H.-D. Meyer, Phys. Rep. **324**, 1 (2000).
[32] *Modern Quantum Chemistry: Introduction to Advanced Electronic Structure Theory*, edited by A. Szabo and N. S. Ostlund (Dover, Mineola, NY, 1996).
[33] C. Lubich, Math. Comput. (to be published).
[34] J. Zanghellini, M. Kitzler, C. Fabian, T. Brabec, and A. Scrinzi, Laser Phys. **13**, 1064 (2003).
[35] J. Zanghellini, M. Kitzler, T. Brabec, and A. Scrinzi, J. Phys. B **37**, 763 (2004).
[36] T. Kato and H. Kono, Chem. Phys. Lett. **392**, 533 (2004).
[37] A. M. Popov, O. V. Tikhonova, and E. A. Volkova, Opt. Express **8**, 441 (2001).
[38] J. M. Feagin and J. S. Briggs, Phys. Rev. A **37**, 4599 (1988).
[39] C. Lubich, Appl. Numer. Math. **48**, 355 (2004).
[40] C. Leforestier and R. E. Wyatt, J. Chem. Phys. **78**, 2334 (1983).
[41] R. Kosloff and D. Kosloff, J. Comput. Phys. **63**, 363 (1986).
[42] U. V. Riss and H.-D. Meyer, J. Chem. Phys. **105**, 1409 (1996).
[43] G. G. Balint-Kurti, R. N. Dixon, C. C. Marston, and A. J. Mulholland, Comput. Phys. Commun. **63**, 126 (1991).
[44] D. J. Tannor and D. E. Weeks, J. Chem. Phys. **98**, 3884 (1993).
[45] W. H. Miller, S. D. Schwartz, and J. W. Tromp, J. Chem. Phys. **79**, 4889 (1983).
[46] M. Lezius, V. Blanchet, M. Ivanov, and A. Stolow, J. Chem. Phys. **117**, 1575 (2002).
[47] M. Kitzler, J. Zanghellini, C. Jungreuthmayer, M. Smits, A. Scrinzi, and T. Brabec, Phys. Rev. A **70**, 041401(R) (2004).
[48] M. Suzuki and S. Mukamel, J. Chem. Phys. **120**, 669 (2004).
[49] M. Beck and H.-D. Meyer, Z. Phys. D: At., Mol. Clusters **42**, 113 (1997).
[50] O. Koch, WSEAS Trans. Math. **3**, 584 (2004).
[51] E. Schmidt, Math. Ann. 433 (1907).
[52] A. Jäckle and H.-D. Meyer, J. Chem. Phys. **109**, 3772 (1998).
[53] A. Jäckle and H.-D. Meyer, J. Chem. Phys. **105**, 6778 (1996).